2013 IEEE/RSJ International Conference on
Intelligent Robots and Systems (IROS)
November 3-7, 2013. Tokyo, Japan

Modeling and Control of A Pneumatic-Electric Hybrid System

Tatsuya Teramae[1], Tomoyuki Noda[1], Sang-Ho Hyon[1 2] and Jun Morimoto[1]

Abstract— **We introduce our Pneumatic-Electric (PE) hybrid actuator model and propose to use the model to derive a controller for the hybrid actuation system by an optimal control method. Our PE hybrid actuator is composed of Pneumatic Artificial Muscle (PAM) and an electric motor. The PE hybrid actuator is light and can generate large torque. These properties are desirable for assistive devices such as exoskeleton robots. However, to maximally take advantage of PE hybrid system, we need to reasonably distribute necessary torque to these redundant actuators by properly taking distinctive characteristics of a pneumatic actuator and an electric motor into account. To do this, in this study, we use an optimal control method called iterative LQG to reasonably distribute the necessary torque to the PAM and the electric motor. The crucial issue to apply the optimal control method to the PE hybrid system is PAM modeling. We built a PAM model composed of three elements: 1) an (air)pressure-force conversion model, 2) a contraction rate model, 3) time delay of the air valve, and 4) the upper limit of force generation that depends on the contraction rate and the movable range. We apply our proposed method to a one degree of freedom (one-DoF) arm with PE hybrid actuator. The one-DoF arm successfully swing tasks 0.5 Hz, 2 Hz and 4 Hz and swing up and stability task by reasonably distributing necessary torque to the two different actuators in a simulated and a real environments.**

I. INTRODUCTION

A light-weight actuator with large torque, high frequency response, precise control accuracy, and high safety is desirable especially for assistive robots. However, the development of such an actuator remains difficult. In our previous research, we proposed combining different kinds of existing actuators to achieve high actuation performance rather than directly developing a single high performance actuator, used the hybrid actuation system for our exoskeleton robot [1] (see Fig. 1 (a)). In concrete, we developed a hybrid actuation system using a Pneumatic Artificial Muscle (PAM), and an electric motor [1]. PAM has strengths: high power-to-weight ratio and inherent compliance provided by the material and the pneumatic. An electric motor also has strengths: high actuation performance in terms of the control frequency bandwidth. For a Pneumatic-Electric (PE) hybrid actuator, the necessary torque to generate a target movement need to be properly distributed to both the PAM and the electric motor. Similar approach is also presented in [8], [9], but this approach considers only torque distribution in snapshot. In our previous study, we proposed using an optimal control method to solve this torque distribution problem and showed preliminary simulation results [3]. In this study, we show the actual control performance of a real one-DoF arm robot which uses the developed PE hybrid actuation system. We use the optimal control method called iterative Linear Quadratic Gaussian (LQG) [5] to distributes the necessary torque to the PAM and the electric motor.

The crucial issue to apply the optimal control method to the real PE hybrid system is PAM modeling. The model need to be constructed by taking specific PAM characteristics into account. Our PAM model consists of four components: 1) an (air)pressure-force conversion model, 2) a contraction rate model, 3) time delay of the air valve, and 4) the upper limit of force generation that depends on the contraction rate and the movable range. The constructed PAM model is used to derive the optimal control strategy for the one-DOF arm robot (see Fig. 1 (b)). To be light weight and minimize energy consumption, exoskeleton robot must be constructed by most basic actuators. One-DoF equip an PAM and small electric motor and does not equip an antagonist PAM. Therefore, in this case, PAM can output positive torque only, and torque cannot be decreased earlier than gravity acceleration. However, assuming stand up/down and walking using exoskeleton robot, the human standing up and lift up motion require the large positive torque, but the human standing down and lift down motion require the small torque can output small electric motor because enough torque is given by gravity. In this study, PAM and motor torque distribution is computed by optimal control considering to limited PAM torque.

We will first introduce our PE hybrid actuator model in Section II. In Section III, we explain how we derive the torque distribution strategy using iterative LQG [5]. Finally, in Section IV, we show control performances of the one-DoF system using our proposed approach.

II. MODELING OF ONE-DOF SYSTEM WITH PE HYBRID ACTUATOR

This section shows modeling of one-DoF system with the PE hybrid actuator. Figure 1 (c) shows that one-DoF system with the PAM and the AC motor with low gear and a current feedback motor driver [4]. The PAM is connected to a pulley using a wire, and the PAM consists of a rubber muscle (FESTO) connected to pneumatic regulation valve system with an air pomp. PAM torque τ_p is generated by force F of PAM contraction transfered through the pulley and wire (tendon). PAM torque τ_p is

$$\tau_p = rF. \tag{1}$$

r is a radius of pulley and constant in this experimental setup

Modeling of PAM is difficult because the PAM has nonlinear characteristics of air and mechanical structure. In this

[1]Department of Brain Robot Interface, ATR Computational Neuroscience Laboratories, Kyoto, Japan

[2]Department of Robotics, Ritsumeikan University, Shiga, Japan

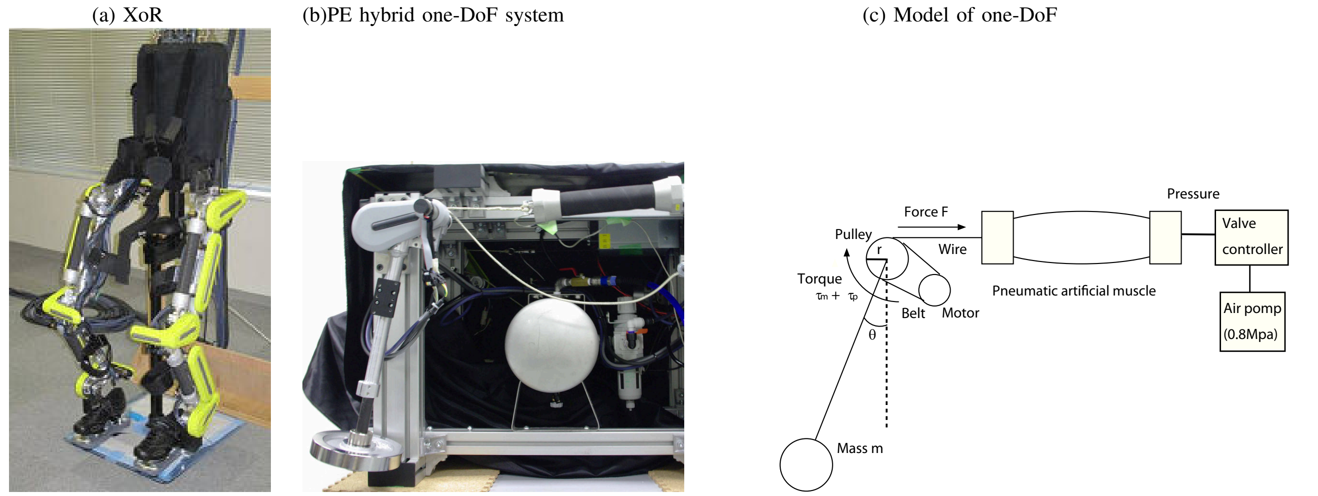

Fig. 1. Exoskeleton robot for lower human body: XoR and One Degree of Freedom(DoF) system: This study aims that the optimal control apply to XoR. One-DoF system is equal to XoR knee joint. In this study, we applied one-DoF to our approach

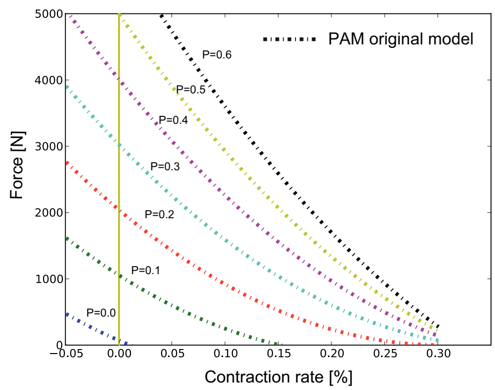

Fig. 2. Quadratic model between force and contraction rate of PAM. In each constant pressure, we fit the virtual data of data sheet provided by FESTO. Those fitting curve has high accuracy for the virtual data.

study, we construct the PAM model by the static model imported the dynamics between pressure and force, the time lag system considered the dynamics between air and pressure and the constraint conditions set as the PAM particular limitation.

A. An air pressure and force conversion model

Figure 2 shows fitting carve based on contraction of PAM and generated force when PAM inner pressure is set as several constant value(0.0–0.6 MPa) [10]. A original statics model between force and contraction to PAM force can be written 2nd order polynomial. There are linear relation between pressure increase and force generation at same contraction rate. The original quadratic model of PAM force is

$$F = \frac{(f_u - f_l)P + P_u f_l - P_l f_u}{P_u - P_l}. \tag{2}$$

f_l is quadratic equation between pressure and contraction of PAM when PAM pressure is set as p_l, and f_u is also quadratic equation when PAM pressure is set as p_u In this study, p_l and p_u are set as 0.2 MPa and 0.7 MPa.

TABLE I
COEFFICIENT IN PRESSURE-CONTRACTION MODEL

a_l, b_l, c_l	22142, -13431, 2031
a_u, b_u, c_u	5426, -32110, 9839

$$f_l = a_l\alpha^2 + b_l\alpha + c_l \tag{3}$$

$$f_u = a_u\alpha^2 + b_u\alpha + c_u \tag{4}$$

Each coefficient is shown in TABLE I. α is contraction rate of PAM calculated by measured joint angle θ.

$$\alpha = \frac{r\theta}{l_{pam}} \tag{5}$$

l_{pam} is length of PAM when pressure is 0. Desired pressure P to generate desired force F is derived based on (2) as follow

$$P = \frac{(P_u - P_l)F - (P_u f_l - p_l f_u)}{f_u - f_l}. \tag{6}$$

B. A construction rate model

However, this original pressure model has a problem that model error is large especially in large force operation [2]. The model error is caused by the wire which connects between the PAM and the pulley, because the wire has initial laxity and extension. So we modeled wire characteristics by tendon-spring model in our previous study[2] with initial laxity. We implemented initial laxity σ to equation (5).

$$\alpha = \frac{r\theta - \sigma}{l_{pam}}. \tag{7}$$

Force of wire extension F^* was set as spring model with equilibrium assumption at desired force.

$$F^* = k\Delta\alpha. \tag{8}$$

k was wire spring coefficient and $\Delta\alpha$ was extra contraction rate by wire extension. Therefore, actual contraction rate α^*

was defined using measured contraction rate α and extra contraction rate $\Delta\alpha$ as follows

$$\alpha^* = \alpha + \Delta\alpha. \tag{9}$$

We fit k and σ using least mean square method based on calibration data (several force, pressure and contraction rate). We can calculate reasonable pressure to generate desired force using α^* in original quadratic model (6).

C. Time delay of the air valve

An air pressure is provided to the PAM by the proportional pressure regulator. Therefore, to compensate air and pressure dynamics by valve response, in this case, the air pressure dynamics is approximated by first order lag system as follows

$$\tau_p(i) = \tau_p(i-1) + \dot{\tau}_p(i)(1 - exp(-\frac{\Delta t}{C})), \tag{10}$$

Where, Δt is sampling time. C is time constant and set as 0.4 s based on the air ejection characteristics in the valve.

D. Constrain conditions

A movable range in the PAM is limited corresponding to the PAM length. The PAM has characteristics that the maximum torque is decreased with increasing the contraction rate like the human muscle. Then, the constraint conditions are set as the maximum torque and the movable range. The movable range can be described as the conditional equation $\tau_p = 0$ when $\theta > \theta_{max}$. Assuming the relation between the maximum torque and the contraction rate is linear, the equation of maximum torque is approximated as follows

$$\tau^{max} = \tau_p^{max}(\theta_{max} - \theta)/\theta_{max} + \tau_p^{base}. \tag{11}$$

We construct the extended PAM model using those models and constraint conditions.

E. Combined PAM model

Next, the state equation of one-DoF system is derived. The state equation of one-DoF system is as follows

$$\dot{\boldsymbol{x}} = \boldsymbol{f}(\boldsymbol{x}, \boldsymbol{u}) = \boldsymbol{A}_{state}\boldsymbol{x} + \boldsymbol{B}_{state}\boldsymbol{u} + \boldsymbol{H}_{extra}. \tag{12}$$

$$\boldsymbol{x} = \begin{bmatrix} \theta & \dot{\theta} & \tau_p \end{bmatrix}^T, \boldsymbol{u} = \begin{bmatrix} \dot{\tau}_p & \tau_m \end{bmatrix}^T$$

Here, θ is joint angle, τ_p is PAM torque and τ_m is motor torque. $\boldsymbol{H}_{extra}$ is extra torques and non-linear terms and, in this case, has gravity term only.

$$\boldsymbol{A}_{state} = \begin{bmatrix} 0 & 1 & 0 \\ 0 & -I^{-1}\mu & I^{-1} \\ 0 & 0 & 0 \end{bmatrix},$$

$$\boldsymbol{B}_{state} = \begin{bmatrix} 0 & 0 \\ I^{-1}(1 - exp(\frac{\Delta t}{C}))\Delta t & I^{-1} \\ 1 & 0 \end{bmatrix}$$

$$\boldsymbol{H}_{extra} = \begin{bmatrix} 0 \\ I^{-1}mgl\sin\theta \\ 0 \end{bmatrix}$$

Model parameters are shown in TABLE II. The inertia I and the joint friction μ was identified using the calibration data of free fall task from $\frac{\pi}{2}$ rad.

TABLE II

MODEL CONDITIONS

Mass(m)	4.2[kg]
Length(l)	0.4[m]
Joint friction(μ)	0.169[Ns/m]
Inertia(I)	0.750[kg/s^2]
Sampling time(Δt)	0.004[s]

III. OPTIMAL TORQUE DISTRIBUTION FOR PE HYBRID ACTUATION SYSTEM

This section shows the iterative Linear Quadratic Gaussian(iLQG) method for one-DoF system with PE hybrid actuator. The iLQG method is optimal control method that reference trajectory and control input is computed by iteratively solving Linear Quadratic Gaussian problem in Δt[5], [6], [7]. iLQG method algorithm is as follows

1) Generation of initial control sequence trajectory.
2) Approximation of dynamics and cost along a trajectory (16)∼(20).
3) Computation of optimal control law and cost-to-go function (14), (15).
4) Generation of new control sequence trajectory and computation of cost in the simulated model described in (12), (13).
5) Update of Learning rate by Levenberg-Marquardt method.
6) If learning rate is minimum, algorithm finish, else, go to step 2).

Each equations are defined as follows. Control input $\boldsymbol{u}$ is given by (13).

$$\boldsymbol{u}_{k+1} = \boldsymbol{u}_k + \dot{\boldsymbol{u}}_k\Delta t \tag{13}$$

k is sampling number. Control law $\dot{\boldsymbol{u}}_k$ is

$$\dot{\boldsymbol{u}}_k = \boldsymbol{l}_k + \boldsymbol{L}_k\Delta t. \tag{14}$$

$$\boldsymbol{l}_k = -\boldsymbol{H}_k^{-1}\boldsymbol{g}_k, \boldsymbol{L}_k = -\boldsymbol{H}_k^{-1}\boldsymbol{G}_k. \tag{15}$$

The shortcuts variable $\boldsymbol{H}, \boldsymbol{G}, \boldsymbol{g}$ are

$$\boldsymbol{H} = \boldsymbol{R}_k + \boldsymbol{B}_k^T\boldsymbol{S}_{k+1}\boldsymbol{B}_k, \tag{16}$$

$$\boldsymbol{G} = \boldsymbol{P}_k + \boldsymbol{B}_k^T\boldsymbol{S}_{k+1}\boldsymbol{A}_k, \tag{17}$$

$$\boldsymbol{g} = \boldsymbol{r}_k + \boldsymbol{B}_k^T\boldsymbol{S}_{k+1}, \tag{18}$$

where, $\boldsymbol{A}_k, \boldsymbol{B}_k$ are defined as follows

$$\boldsymbol{A}_k = \boldsymbol{I}_n + \Delta t\frac{\partial \boldsymbol{f}}{\partial \boldsymbol{x}}, \boldsymbol{B}_k = \Delta t\frac{\partial \boldsymbol{f}}{\partial \boldsymbol{u}}.$$

$\boldsymbol{f}$ is state equation (12), J is objective function when k, $\boldsymbol{x}$ is state variable, $\boldsymbol{u}$ is input, and $\boldsymbol{r}_k, \boldsymbol{R}_k$ are

$$\boldsymbol{r}_k = \Delta t\frac{\partial J_k}{\partial \boldsymbol{u}}, \boldsymbol{R}_k = \Delta t\frac{\partial^2 J_k}{\partial \boldsymbol{u}\partial \boldsymbol{u}}.$$

$\boldsymbol{P}_k$ is

$$\boldsymbol{P}_k = \Delta t\frac{\partial^2 J_k}{\partial \boldsymbol{u}\partial \boldsymbol{x}}.$$

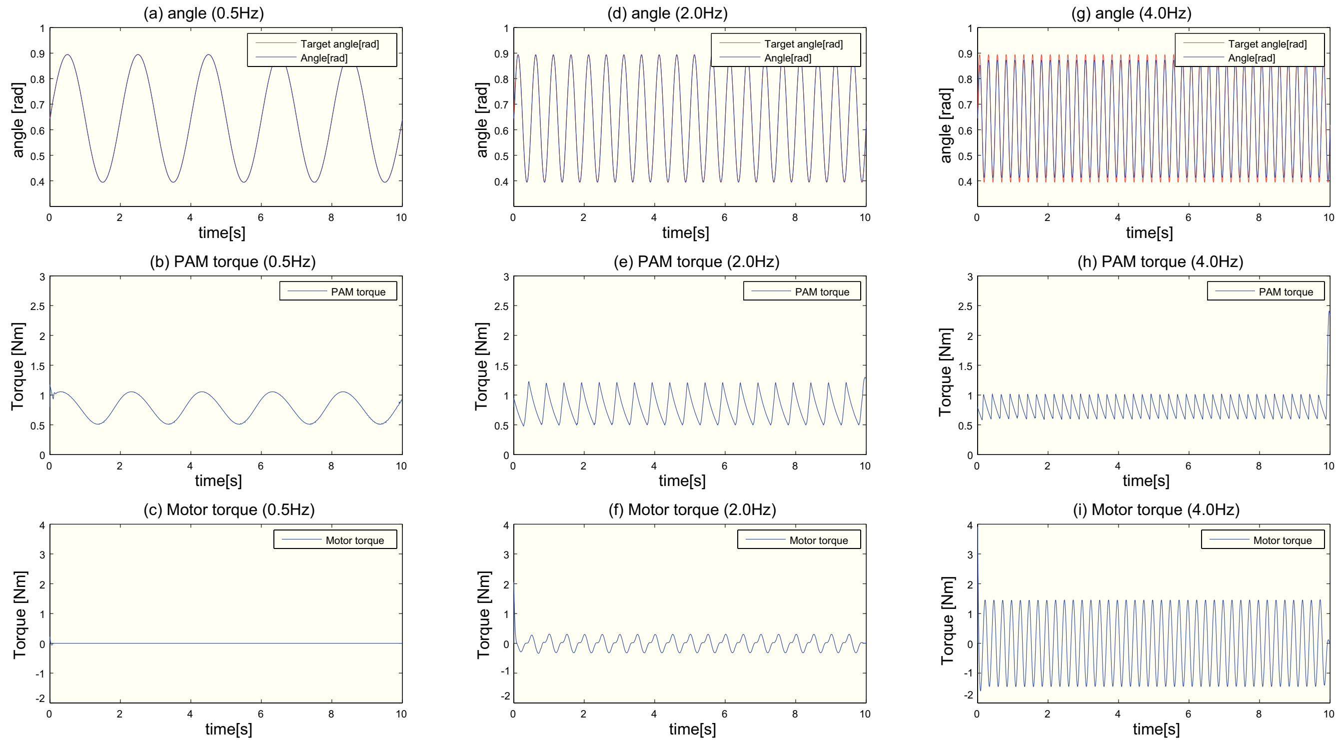

Fig. 3. Simulation results of swing task. horizontal axis is time, vertical axis is torque or angle. blue line show angle, PAM torque and motor torque. Red line shows target angle. (a)∼(c) are results of 0.5 Hz. (d)∼(f) are results of 2.0 Hz. (g)∼(i) are results of 4.0 Hz. Simulation conditions: Experimental duration is 10[s]. Sampling frequency is 250[Hz]. Reference trajectory set as $0.644 + 0.25\sin(2\pi f t)$. f is frequency and t is time. Objective function weights are $w_p = 10^5$, $w_v = 0$, $w_{pn} = 10^{-7}$, $w_m = 200$

The cost-to-go parameters $\boldsymbol{S}_k, \boldsymbol{s}_k$ are represented as

$$\boldsymbol{S}_k = \boldsymbol{Q}_k + \boldsymbol{A}_k^T \boldsymbol{S}_{k+1} \boldsymbol{A}_k - \boldsymbol{G}^T \boldsymbol{H}^{-1} \boldsymbol{G}, \tag{19}$$

$$\boldsymbol{s}_k = \boldsymbol{q}_k + \boldsymbol{A}_k^T \boldsymbol{S}_{k+1} - \boldsymbol{G}^T \boldsymbol{H}^{-1} \boldsymbol{g}, \tag{20}$$

where $\boldsymbol{q}_k, \boldsymbol{Q}_k$ are

$$\boldsymbol{q}_k = \Delta t \frac{\partial J}{\partial \boldsymbol{x}}, \boldsymbol{Q}_k = \Delta t \frac{\partial^2 J}{\partial \boldsymbol{x} \partial \boldsymbol{x}}.$$

IV. Verification of Optimal Control for PE Hybrid System

We evaluate our optimal control approach for PE hybrid actuator by the numerical simulation and the experiment using one-DoF system. In the simulation, the PAM and the motor torques distribution was computed by iLQG method based on objective function and the reasonability of torque distribution was verified. In the experiment, one-DoF system was controlled by feed-forward control using input torque computed by simulation. The accuracy of constructed model and position control in one-DoF system with PE hybrid actuator is verified by experimental results.

A. Simulation

Simulation task is sin wave trajectory (0.5 Hz, 2 Hz and 4 Hz) to validate the performance of our approach. PAM and motor torques are optimized to minimize energy consumption. An energy consumption in motor can be optimized by minimizing torques. We also assume minimizing torque for cost related to PAM torque, and this study investigates the relation between the frequency of target trajectory and the torque distribution using the optimal control framework. Therefore, the objective function is set as follows

$$\begin{aligned} J \;\; &= \;\; \int_0^{t_f} \{ w_p(\theta - \theta_{ref})^2 + w_v(\dot{\theta} - \dot{\theta}_{ref})^2 \\ &+ \;\; w_{pn}\tau_p^2 + w_m \tau_m^2 \} dt. \end{aligned} \tag{21}$$

The objective function optimizes summation of motor torque τ_m and PAM torque τ_p. This also minimizes the error between the joint angle and the target angle θ_{ref}, and between the joint angular velocity and the target angular velocity $\dot{\theta}_{ref}$.

Figure 3 shows the simulation conditions and results. Figure 3 (a), (d) and (g) show that angle can follow target angle in each tasks. Figure 3 (b) and (c) show that PAM dominantly output the torque. Figure 3 (e) and (f) show that PAM increases the torque when the positive angular velocity is required and the motor output the torque when the negative angular velocity is required, because the PAM torque cannot follow the negative angular velocity by the air ejection characteristic that decreasing torque is limited less than gravity acceleration. Figure 3 (h) and (i) also show that PAM covers positive angular velocity and motor covers negative angular velocity, moreover, motor dominantly output the torque, because the frequency of target trajectory is high. If PAM output large torque, PAM torque cannot decrease to the reasonable torque. However, figure 3 (h) shows that

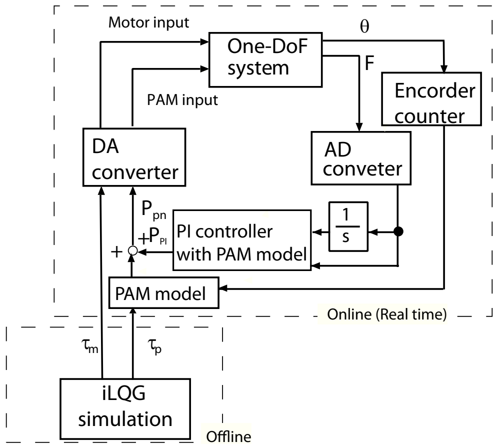

Fig. 4. Block diagram in experiment

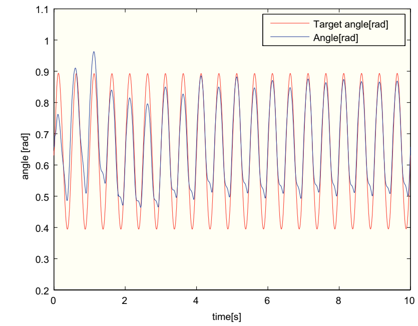

Fig. 5. Experimental results of swing task 2 Hz. horizontal axis is time, vertical axis is angle in (a) and torque in (b) and (c). Blue line set as measured value and red line set as reference value. Experimental conditions: Experimental duration is 10s, sampling frequency is 250 Hz, target trajectory set as 2 Hz sin wave, real-time OS used Debian 6 with Xenomai 2.5.2, real-time networking used RTnet 0.9.13, I/O device used Multi Function Board equipped with LAN port, AD converter, DA converter, encoder counter and DIO

PAM output large torque in last time around 10 s. Because, it is not necessary that PAM torque is decreased. PAM that energy cost is low dominantly output the torque.

Therefore, the PAM and motor torques were reasonably distributed based on frequency of target trajectory and each actuators characteristics by our approach.

Next, the torque in Figure 3 (e) and (f) were applied to the actual one-DoF system and the accuracy of structured model and torque distribution were verified in the experiment.

B. Experiment

Figure 4 shows a block diagram of the experimental flow using one-DoF system. The air pressure input P_{pn} for PAM is computed by (6) based on the desired force F computed by desired torque τ_p in the simulation and the contraction rate computed by measured angle in the experiment. The PAM input set as feed-forward input P_{pn} and PI control input P_{PI} by the error between the desired torque and measured torque. PI controller is pressure controller to follow the reference torque input computed by iLQG. Motor input is the desired torque τ_m in the simulation. The system output (joint angle and force) is measured by the encoder and load cell. In the experiment, the I/O signal communication between control PC and one-DoF system is realized by hard real-time UDP protocol using Debian 6.0 with Xenomai and RTnet. Xenomai is real-time kernel patch for Linux and RTnet is hard real-time networking for Xenomai.

Figure 5 shows the experimental results and conditions and the joint angle was following target angle in actual system. However, error between measured angle and target angle was maximally 0.1 rad. This error cause the PAM pressure model error. We suppose that this error can be improved by modification of PAM pressure model. However, this result suggests that our approach can control position with high accuracy by only feed-forward input computed by iLQG. Moreover, it could be verified that the accuracy of structured model was high, because measured angle follows target trajectory by feed-forward torque input only.

Next, the task is set as swinging up and stability on top with heavy weight(2.5 kg). We set the task that cannot achieve by only motor or PAM. The objective function set as follows

$$J_{swing} = w_p(\theta_{t_f} - \theta_{ref})^2 + w_v(\dot{\theta}_{t_f} - \dot{\theta}_{ref})^2 + \int_0^{t_f} \left\{ w_{pn}\tau_p^2 + w_m\tau_m^2 \right\} dt. \quad (22)$$

The objective function optimizes the error between the joint angle in final state and the target angle θ_{ref}, and between the joint angular velocity in final state and the target angular velocity $\dot{\theta}_{ref}$. In actual system, movable range of joint and control range in PAM are limited due to PAM length. Then, the objective function J_p is used when $\theta < 0$.

$$J_p = J + \int_0^{t_f} w_d\theta^2 dt (\text{if } \theta < 0) \quad (23)$$

w_d is penalty weight for limited joint angle. In this case, we give only the target angle and velocity in final state to the optimal control, and we compute the reference trajectory and the distribution of PAM and motor torque to follow the reference trajectory using iLQG. The PAM input is set as feed-forward input P_{pn}. Motor input is summation of desired torque τ_m in the simulation and the state feedback control input torque τ_{lqr} using LQR for stability of arm.

Figure 5 shows the simulation and experimental results and conditions of swinging up and stability task. Figure 7 shows the movement of one-DoF system that divided 6 pictures from 0 s to 1.5 s. Figure 6 (a) shows that the PAM output the necessary large torque to reach to around π rad when joint angle was around 0 rad that PAM could output large torque. The motor controlled joint angle to reach to the target angle and the target angular velocity in final state by low torque when angle was around π rad that PAM could not use a torque and necessary torque was low. Therefore, our approach could realize the task that cannot achieve by only motor or PAM.

Figure 6 (b) shows that the joint angle was also following reference trajectory in actual system. the error between actual angle and target angle in final state was 0.059 rad. the error

(a) Simulation results (b) Experimental result

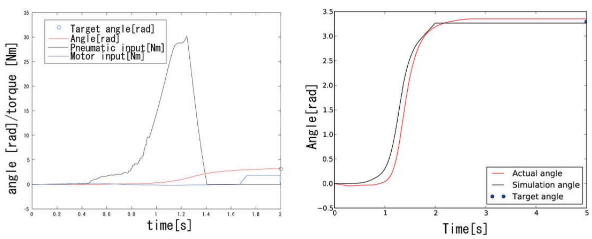

Fig. 6. Results of swinging up and stability on top task. Horizontal axis set as time, vertical axis as set angle/torque in (a) and angle in (b). In (a), red line, black line, blue line and circle set as angle, PAM torque, motor torque and target angle in final state. In (b), red line, black line and circle set as measured angle, reference trajectory and target angle in final state. Conditions: Experimental duration is 5[s], sampling frequency is 250[Hz], initial angle, target angle, and target velocity are 0 deg, 180 deg, and 0[deg/s], objective function weights are $w_p = 10^5$, $w_v = 10^3$, $w_{pn} = 10$, and $w_m = 300$, PAM movable range is set as $0 < \theta < \frac{\pi}{2}$, PAM torque range used (11), $\tau_p^{max} = 50, \tau_p^{base} = 20$, $\theta_{max} = \frac{\pi}{2}$.

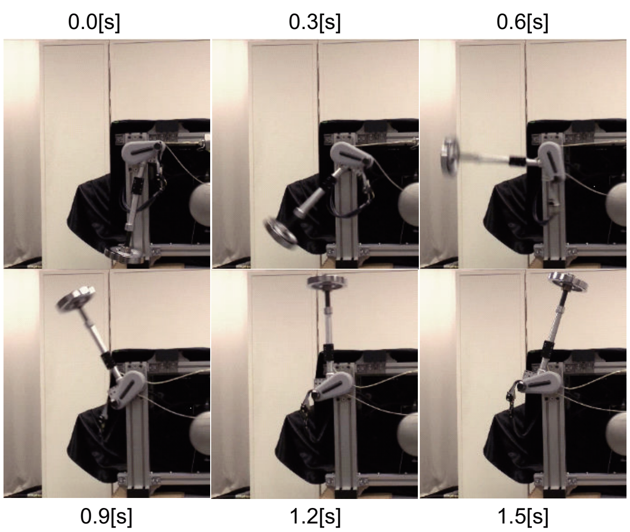

Fig. 7. Experimental results in one-DoF system swing up and stability task

between actual angular velocity and target angular velocity in final state was 0.0 rad/s. the mean of error between the reference trajectory and the measured angle was 0.106 rad. The accuracy of position control is enough to stabilize one-DoF system on top with PE hybrid actuator and limited control range. Therefore, it was verified that the accuracy of structured model was reasonable.

V. Conclusion

This study aimed that PAM and motor torque is reasonably distributed and position control with high accurate using the optimal control in one-DoF system with PE hybrid actuator. We constructed PAM model by static model between pressure and force, time lag system in air valve ejection characteristics and constraint conditions of PAM torque limitation. We applied iLQG method to PE hybrid actuation system using the structured model. We verified that PAM and motor torque could be reasonably distributed by optimal control in the simulation results. The accuracy of position control were verified by the experimental results using one-DoF system. We also confirmed that the approximated model derived by the original force and pressure model and torque limitation as constraint conditions was reasonably achieved swing trajectory and swing up motion. In future works, we will improve the model by implementing wire laxity characteristics, and we will try that state equation will extend to 3 link model and apply the proposed method to the exoskeleton robot.

Acknowledgments

We thank Takamitsu Matsubara for initiating this study. We thank Nao Nakano, Akihide Inano, Junnichiro Furukawa and Naoki Honnma for hardware maintainance and helping our experiments. This study is the result of SRPBS, MEXT. This work was also supported by the Strategic International Research Cooperative Program, Japan Science and Technology Agency (JST). The work of J. Morimoto was supported by the MEXT KAKENHI under Grant 23120004. This work was also supported by JSPS and MIZS under the Japan-Slovenia Research Cooperative Program. T. Noda was partially supported by KAKENHI Grant Number 24700203.

References

[1] S.H. Hyon, J. Morimoto, T. Matsubara, T. Noda, and M. Kawato, ”XoR: Hybrid Drive Exoskeleton Robot That Can Balance,” in Proceedings of the IEEE/RSJ Intl. Conference on Intelligent Robots and Systems, 2011

[2] T. Noda, N. Sugimoto, J. Furukawa, M. Sato, S. H. Hyon, J. Morimoto, ”Brain-Controlled Exoskeleton Robot for BMI Rehabilitation, 12th IEEE-RAS International Conference on Humanoid Robots, pp. 22–27, 2012.

[3] T. Matsubara, T. Noda, S. H. Hyon, J. Morimoto, ”An Optimal Control Approach for Hybrid Actuator System,” 2011 IEEE-RAS International Conference on Humanoid Robots, pp. 300–305, 2011.

[4] T. Noda, J. Furukawa, T. Teramae, S.H. Hyon, and J. Morimoto, ”An Electromyogram based Force Control Coordinated in Assistive Interaction,” in Proceedings of the IEEE/RSJ Intl. Conference on Intelligent Robots and Systems (Accepted)

[5] E. Todorov and W. Li, ”A generalized iterative LQG method for locally-optimal feedback control of constrained nonlinear stochastic systems,” In Proceedings of the American Control Conference, pp. 300–306, 2005.

[6] D. Mitrovic, S. Klanke, and S. Vijayakumar, ”Adaptive Optimal Feedback Control withLearned Internal Dynamics Models,” From Motor Learning to Interaction Learning in Robots Studies in Computational Intelligence Volume 264, pp. 65–84, 2010.

[7] D. Mitrovic, S. Klanke and S.Vijayakumar, ”Learning impedance control of antagonistic systems based on stochastic optimization principles,” The International Journal of Robotics Research 30(5), pp. 556–573 2011.

[8] D. Shin, I. Sardellitti, Y.-L. Park, O. Khatib, and M. Cutkosky, ”Design and control of a bio-inspired human-friendly robot,” International Journal of Robotics Research, vol. 29, no. 5, pp. 571–584, 2010.

[9] D. Shin, I. Sardellitti1, O. Khatib, ”A Hybrid Actuation Approach for Human-Friendly Robot Design,” Proceedings of the 2008 IEEE International Conference on Robotics and Automation 2008.

[10] FESTO, http://www.festo.com